Available online at www.sciencedirect.com
ScienceDirect
Trans. Nonferrous Met. Soc. China 35(2025) 499−510
Transactions of Nonferrous Metals Society of China
www.tnmsc.cn

High-temperature fatigue cracking mechanism and microstructure evolution of aero-engine K4169 superalloy in service process

Song-jun WANG[1], Jian-jun HE[1], Zhi-hui GONG[2], Wei-ping LI[2],
Jun-gang YANG [3], Ya-jun SHAO [3], Yu-hui CAI[1], Yue-xin DU[1], Cheng-wei YANG[1]

1. School of Energy and Power Engineering, Changsha University of Science and Technology, Changsha 410114, China;
2. College of Mechanical and Vehicle Engineering, Hunan University, Changsha 410082, China;
3. AECC South Industry Co., Ltd., Zhuzhou 412002, China

Received 3 July 2023; accepted 16 April 2024

Abstract: By using fatigue crack propagation testing and microstructural characterization, the crack fracture and propagation mechanisms of K4169 superalloy under various loads were investigated. The results demonstrate that the grain sizes of K4169 superalloy significantly increase, and the precipitation of the needle-like δ phase and the Laves phase is observed. Voids and microcracks form at location of Laves phase enrichment, creating conditions for crack propagation. By the a−N (a is the crack length, and N is the number of cycles) relationship curve, the change in the fatigue crack growth rate with the increasing number of cycles progresses through three separate stages. The fracture process of K4169 superalloy under low-stress cyclic loading (3 kN) exhibits the ductile fracture. Subsequently, the fracture process starts to change from the ductile fracture to the brittle fracture as the stress increases to 4.5 kN. In the microstructures of fractures in both stress states, intergranular propagation is the mechanism responsible for crack propagation. Moreover, the Laves phase exists near the fracture crack, which is in line with the post-service structural phenomenon.

Key words: K4169 superalloy; high-temperature fatigue; microstructure; crack propagation; aero-engine

1 Introduction

High-temperature (reaching 700 °C) hot-end components are typically composed of the high-strength nickel-based alloy K4169. This alloy, which is widely applicable in the aerospace industry, is formable and has excellent mechanical characteristics and a high fatigue resistance [1−3]. When driving the aero-engine, the components are usually subjected to high temperatures and prolonged operation time. The hot-end components are held under harsh conditions, such as high temperatures and heavy loads, for extended periods of service [4−6]. The hot-end components crack as a result of the severe environment until they eventually fail. The microstructure of the K4169 superalloy consists of five distinct phases: γ-Ni-Fe, γ'-Ni_3AlTi, γ''-Ni_3Nb, δ-Ni_3Nb, Laves-Fe_2Nb and MC carbides. The plate-shaped γ'' phase is the primary and thermodynamically metastable phase. However, when subjected to high temperatures, this phase transitions into the δ phase, which significantly reduces the performance of the alloy [7−10]. The Laves phase is a common brittle phase in alloys that can cause cracking when subjected to high temperatures, thus significantly reducing the mechanical properties of the alloy [11].

Corresponding author: Jian-jun HE, Tel: +86-15873158505, E-mail: hejianjun@csust.edu.cn
DOI: https://doi.org/10.1016/S1003-6326(24)66695-1

Inconel 718 is a foreign grade K4169 superalloy. Currently, the K4169 superalloy is still under exploration, but Inconel 718 has been the subject of numerous studies on fatigue. According to KONEČNÁ et al [12], fatigue cracks in Inconel 718 alloy spread out in a grain-penetrating manner. The intergranular disruption phase primarily stops the expansion of crystal penetration [13]. The crack propagation mechanism changes with increasing crack propagation rates. In addition, the grain orientation influences the local direction of fracture extension. According to BACHE et al [14], cracking along the crystal in Inconel 718 results in faster crack propagation than cracking through the crystal. Simultaneously, intergranular cracking is triggered by the grain boundary embrittlement; however, the specific process involved remains ambiguous. According to JEONG et al [15], the transition from small-grain cleavage fracture to large-grain striation fracture is the result of the high-temperature fatigue crack propagation mechanism of Inconel 718 alloy in the low ΔK (ΔK is the stress intensity factor range) area. Furthermore, the fatigue crack propagation mechanisms of small and large grains at low ΔK values have been proposed. RASHKOVETS et al [16] discovered that fatigue cracks are predominantly formed by Laves-phase and δ-phase particles. Therefore, effectively eliminating the Laves phase and δ phase through experimentation has been an underlying issue of research. In this context, WAN et al [17] eliminated the Laves phase by applying heat treatment. The fatigue strengths of the γ'/γ'' enhanced phase precipitates substantially increase. Furthermore, the fatigue crack growth process of the alloy is correlated with the distributions of inclusions and grain size at an operating temperature [18]. Moreover, the grain size of an alloy increases the ratio of the fracture initiation life to the total fatigue life [19]. Similarly, YAZDANPANAH et al [20] studied stress corrosion cracking and demonstrated a large dislocation density close to the grain boundaries. Consequently, the main mechanism for the appearance of fractures close to the subgrain boundary is that cracks appear along the grain boundaries and the notched surface slip zone. As a result, as the grain size increases, the crack budding site may change from an intercalation zone to a continuous slip zone. However, there are few investigations on the properties of K4169 superalloys, and little research has been performed on the variations in the grain size during engine maintenance.

Based on an analysis of the service cracking phenomena in the hot-end components of aero-engine, the microstructural changes in samples before and after service, as well as the evolution of grain size and characteristics of precipitated phases throughout their operational lifespan, were explored. High-temperature cyclic loading tests were replicated under two stresses (3 and 4.5 kN) on the materials used in aero-engine. The crack initiation process in K4169 superalloy and the correlation between several cycles and the fatigue crack propagation rate were thoroughly studied under a variety of cyclic loading. Furthermore, micro-structural characterization of the samples subjected to high-temperature stress cyclic loading was conducted. The crack development process provided a qualitative analysis, and the cracking propagation pattern of nickel-based alloy K4169 was summarized. In this study, a framework for safe aero-engine operation was provided.

2 Experimental

2.1 Materials

The experimental materials were acquired from a company that produced after-service test components from a turbine cassette. Figure 1 shows a schematic diagram of the components. The aircraft engine turbine magazines were composed of K4169 superalloy, which primarily comprised Ni, Cr, Fe, Nb, Mo, Ti, and Al. Table 1 presents the

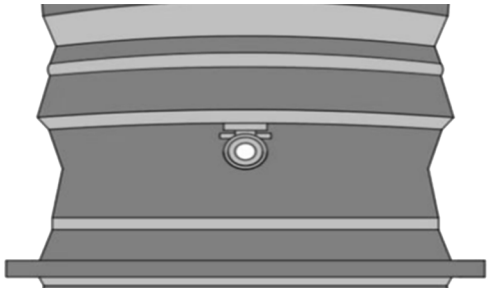

Fig. 1 Schematic diagram of turbine cassette

Table 1 Chemical composition of K4169 superalloy (wt.%)

Ni	Cr	Fe	Nb	Mo	Ti	Al
50.3	20.5	18.4	4.7	2.8	2.2	1.1

chemical composition of the K4169 superalloy that is utilized in this study.

2.2 Method

Test pieces involving the decommissioning of aero-engine hot-end components were prepared. Abrasive pastes with particle sizes of 1 and 0.5 μm were used to polish the surfaces of the decommissioned samples using a polishing machine and emery paper reaching a grade of 2000. When the samples were examined under a Zeiss light microscope, no scratches were observed. Afterward, the grain boundaries of the crystals and a portion of the precipitated phase could be observed by using 10 mL C_2H_5OH + 10 mL HCl + 1.5 g $CuCl_2$.

The fatigue crack propagation test for the fatigue crack propagation rate test was conducted using an electrohydraulic servo fatigue tester. The compact tension (CT) sample with a thickness of 5 mm was composed of K4169 superalloy. The sample had a U-shaped crack that was manufactured with dimensions of 1.6 mm in width and 9 mm in length. Figure 2 shows the geometric dimensions.

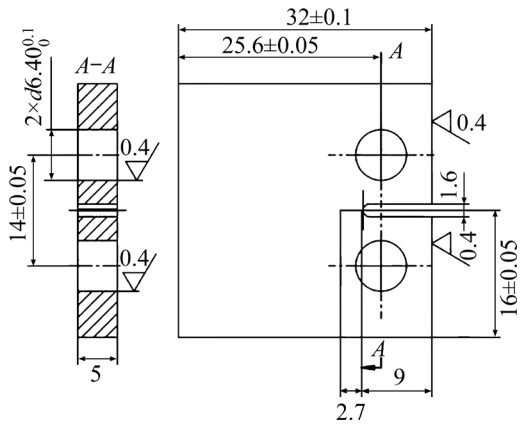

Fig. 2 Schematic size of CT sample (Unit: mm)

To simulate the service environments of the hot-end components of the aero-engine at high temperatures, the fatigue tests were performed on CT samples at 650 °C. To measure and regulate the temperature during testing in high-temperature environments, thermocouples were used to contact with the sample surface. After starting the program to heat the sample to 650 °C for 30 min, the loads for the two sets of crack propagation tests were set to be 3 and 4.5 kN, respectively. The loading frequency was 20 Hz, the stress ratio was 0.06, and the load waveform resembled a sine wave. Simultaneously, the fatigue fracture mechanism of the K4169 superalloy was investigated using SEM. The cracking mechanism was thoroughly examined by EBSD. The CT sample was split into 10 mm × 10 mm × 5 mm cuboids. The sample surfaces were polished to a grade of 2000 using emery paper. Abrasive pastes with particle sizes between 1 and 0.5 μm were used for polishing on a polishing machine. The sample was ultimately exposed to electrolytic corrosion. For electrolytic polishing, the temperature was −20 °C, the voltage was 30 V, and the current was approximately 0.2 A. The electrolytic polishing solution consisted of 20 vol.% $HClO_4$ + 80 vol.% C_2H_5OH.

3 Results

3.1 Microstructural changes of K4169 superalloy before and after service

Metallographic observation was performed on the samples to obtain a complete understanding of the microstructural changes in the parts before and after service. Figure 3 shows the OM images of K4169 superalloy before and after service. The surface of the alloy exhibits a fairly homogenous grain distribution and an equally scattered precipitated phase before it is utilized. Once the sample is sent into service, its grain size increases by approximately three orders of magnitude. The precipitated phases are spread uniformly at the grain boundaries.

The samples were subjected to EBSD and SEM analysis to determine the changes in the grain sizes before and after service. As shown in Fig. 4, the grain orientation map produced by EBSD scanning was used to examine the differences in the grains of the K4169 superalloy samples before and after service. The average grain size of each sample was computed, and Fig. 5 shows the size data. Following service, a significant movement is observed at the sample grain boundary in the direction opposite to *X* axis. The high-temperature tension in the alloy causes the grain to rotate in the direction of the stress when it is used. The samples show no discernible grain alterations before service. However, after service, the sample grain sizes are different. In as many as 35% of instances, individual grains are greater. The large stress concentrations and considerable grain boundary deformations associated with this phenomenon

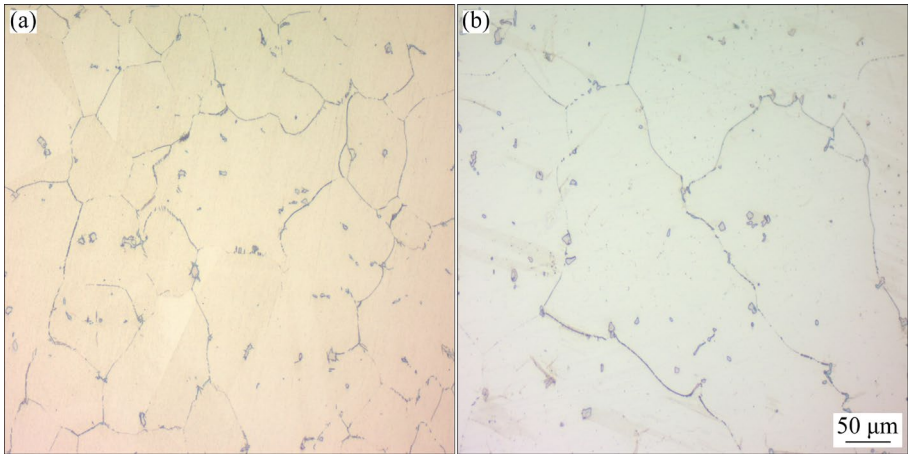

Fig. 3 OM images of K4169 superalloy before (a) and after (b) service

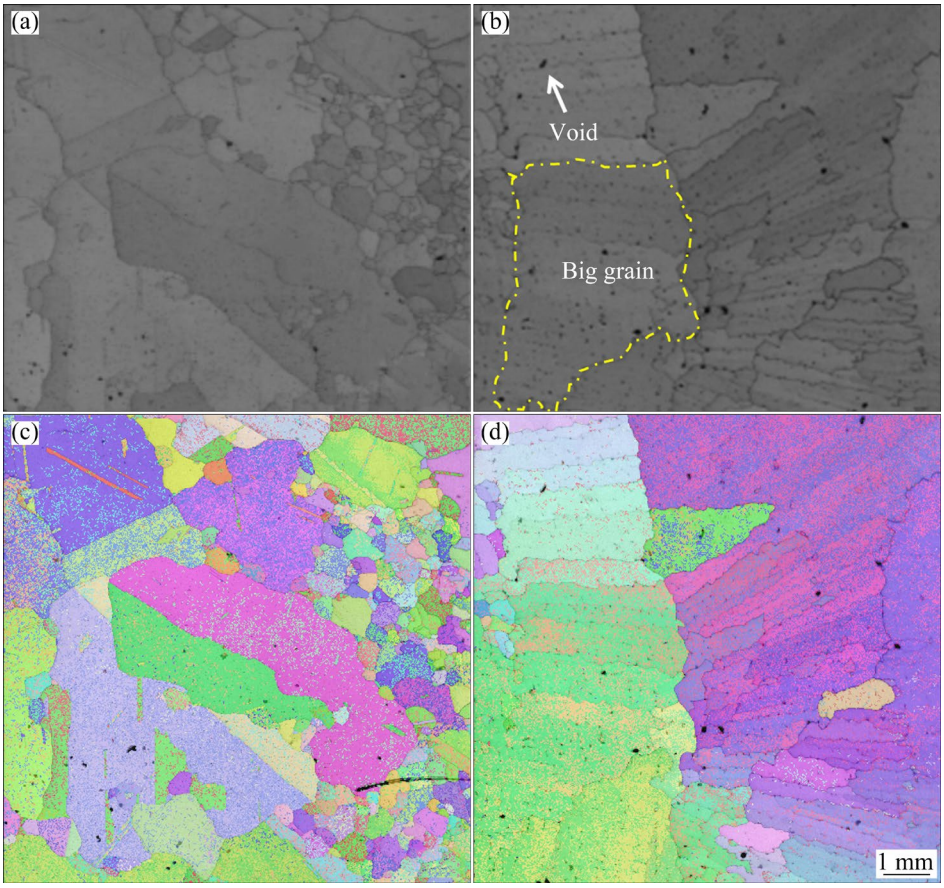

Fig. 4 Microstructural evolution of K4169 superalloy: (a) SEM image before service; (b) SEM image after service; (c) IPF map before service; (d) IPF map after service

promote the production of fatigue cracks. Throughout the offset process, the grains develop several voids along the grain boundaries, as shown in Fig. 4(d). These voids make it possible for the alloy to crack during operation, resulting in component failure.

To understand the changes in the precipitated phases after service, interface morphology analysis was carried out on the post-service samples. The results are shown in Fig. 6. A few voids and microcracks are observed on the surface of the part emerging after service, and the locations where voids and microcracks originate are mostly at the Laves phase. Voids and microcracks originate from the brittle Laves phase of the alloy under high-temperature stress. The needle-like δ phase

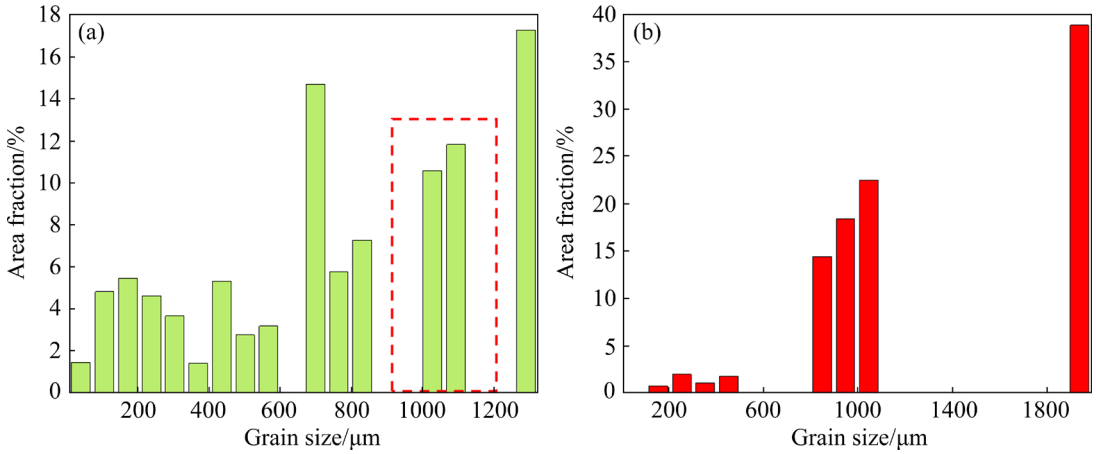

Fig. 5 Grain size distributions of samples before (a) and after (b) service

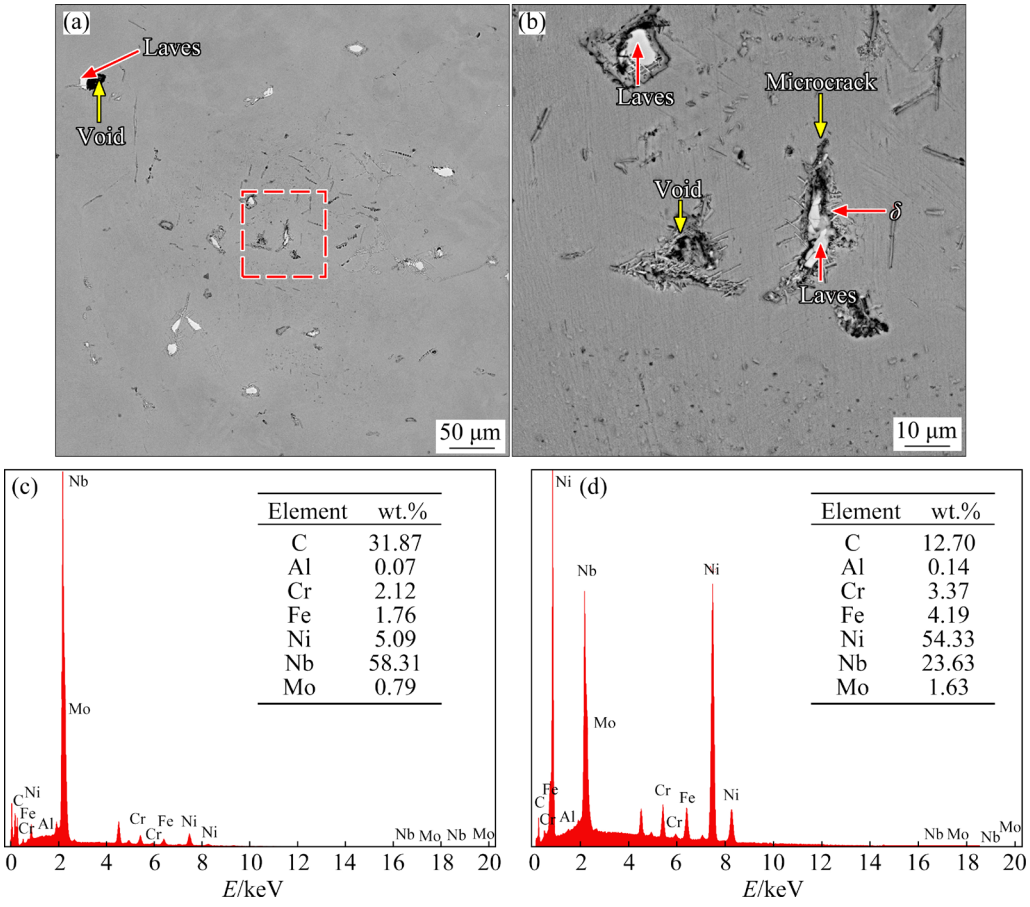

Fig. 6 Interface morphologies of sample after service: (a, b) SEM images of service part; (c) EDS data of Laves phase; (d) EDS data of δ phase

precipitates around the Laves phase (Fig. 6(b)). The precipitation of the δ phase enhances the fatigue resistance of the alloy at 650 °C [21]. When the $\delta(Ni_3Nb)$ precipitated phase is distributed parallel to the Laves phase in a long strip inside the grain, it forms a Weiss structure. This structure can significantly decrease the hardness and strength of the alloy [22].

3.2 Crack propagation fracture behavior

The CT samples undergo prefabricated crack propagation under high-temperature cyclic loading at 3 and 4.5 kN. The crack propagation paths of the samples are presented in Fig. 7.

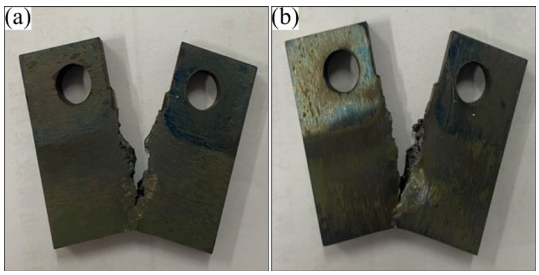

Fig. 7 Physical diagrams of crack propagation paths under different cyclic loadings: (a) 3 kN; (b) 4.5 kN

The crack propagation depths of the samples under the two stresses are almost identical, as shown in Fig. 7. Conversely, the fracture patterns of the CT samples are relatively complex when subjected to 4.5 kN of stress. Following crack propagation, the samples are subjected to EBSD tests (as shown in Figs. 8 and 9), to determine the orientations of the cracks in the grains.

Figures 8 and 9 show that under both cyclic loading conditions, a secondary crack propagation process occurs along the crack propagation fracture. Multisource cracking is not observed in the CT sample. Cracks with different directions of expansion start to appear at the notches on the surface of the piece, and many microvoids form at the ends of the cracks. These voids tend to interact with small fatigue cracks under stress and become the sources of new cracks. In particular, the microstructure exhibits this phenomenon under high-stress cyclic loading. Furthermore, the grains in the crack propagation zone of the CT sample grow notably larger than those in the other locations upon application of a stress load. Therefore, this phenomenon is in line with the microscopic characterization of post-service sample.

Fractures are visible in the grain under both stress loading conditions. Secondary cracking occurs when multiple main fractures form simultaneously across grains with different grain orientations. As shown in Figs. 8(b, c), a sample tends to exhibit crack growth at the interior grain boundaries, and the fracture width is small. The dislocation that occurs during crack propagation is not sufficiently depicted by the KAM diagram (Fig. 8(d)).

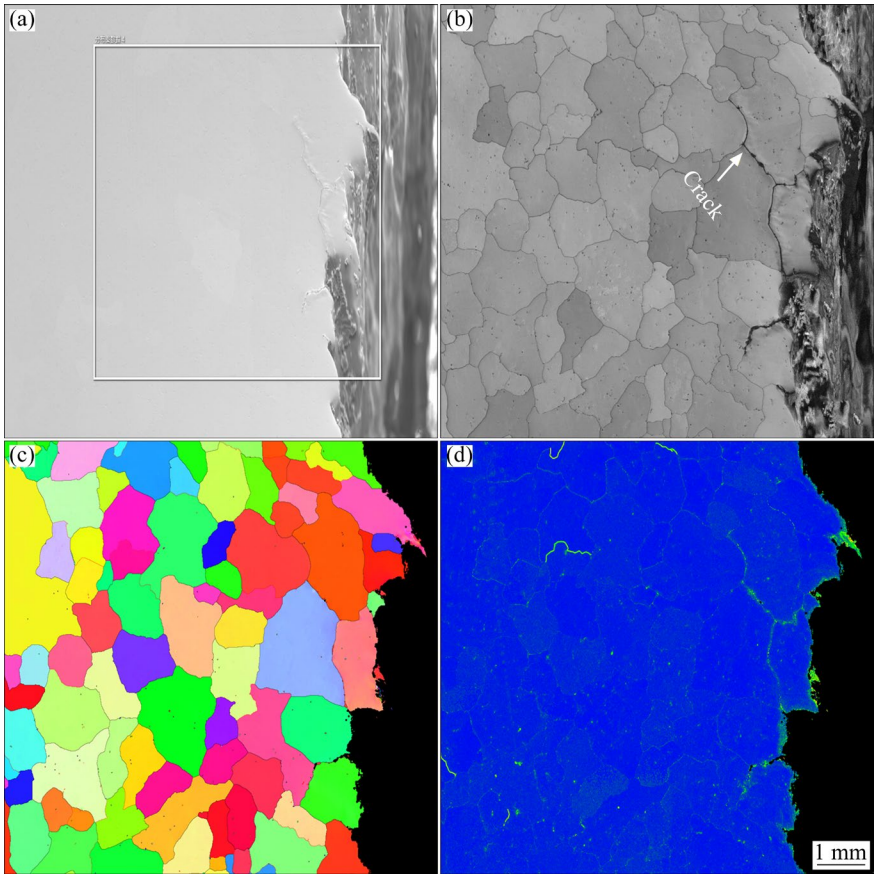

Fig. 8 EBSD analysis maps at fracture of sample under 3 kN cyclic loading: (a) Scan position; (b) Band contrast map; (c) IPF map; (d) KAM map

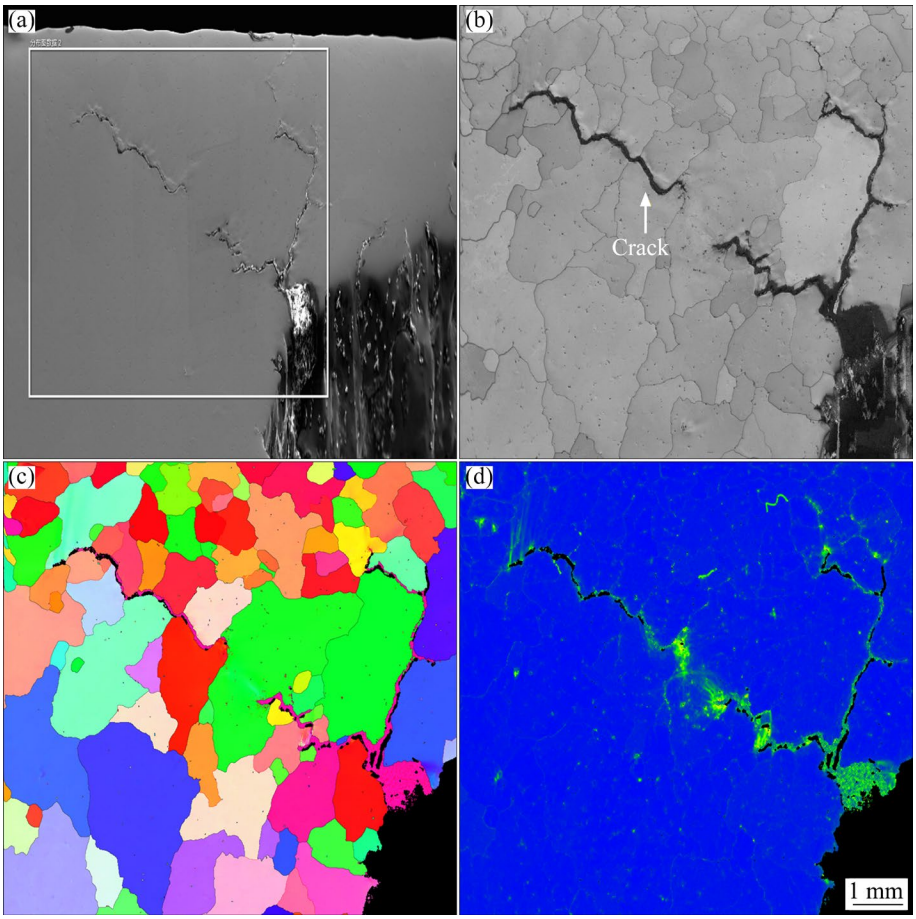

Fig. 9 EBSD analysis maps at fracture of sample under 4.5 kN cyclic loading: (a) Scan position; (b) Band contrast map; (c) IPF map; (d) KAM map

The fractures propagate through the grains in the microstructure under the cyclic loading of 4.5 kN (Figs. 9(b, c)). This finding illustrates the mechanism by which the natural stress in a grain can prevent a crack from growing as the crack moves through the grain. According to Fig. 9(d), the deepest fissures are visible at the crack growth site. As the crack propagates into the grain, the fissures stop growing and become narrower. The KAM diagram shows that at a crack growth site, there is a substantial concentration of dislocations; as the crack widens, this dislocation phenomenon decreases, and the fracture stops expanding.

3.3 Cracking characteristics of K4169 superalloy under high-temperature fatigue

Figure 10 shows the a–N (a is the crack length, and N is the number of cycles) relationship curves of K4169 superalloy under different cyclic loadings. There are three distinct phases in the variation in the fatigue crack propagation rate with an increasing number of cycles.

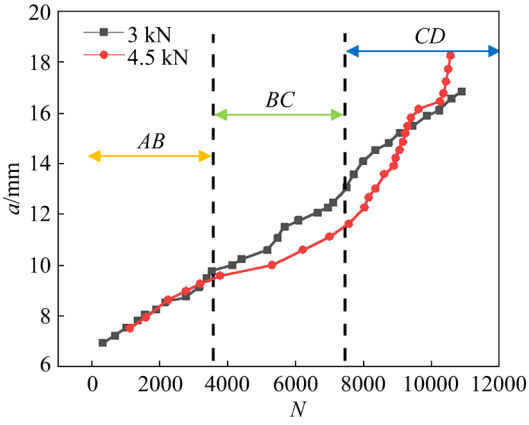

Fig. 10 Crack propagation curves (a–N curves) of samples under different cyclic loadings

According to Fig. 10, under the 3 kN cyclic loading, the a–N curve increases steadily until the fracture stops. Under the 4.5 kN cyclic loading, the a–N curve reflects the first step of the AB stage. The material does not deform significantly during the first stretching stage since it is in a state of elastic deformation and the cyclic loading increases. However, when the cyclic loading exceeds the yield

strength of the material, the material begins to bend plastically, which can cause the alloy to fracture. This phase is frequently denoted as the *BC* stage or stable growth stage. Subsequently, when the applied cyclic loading reaches the tensile strength of the material, the alloy enters the destabilization and expansion stage, which eventually leads to the decomposition of the material, i.e., the *CD* stage [23].

The fatigue fracture microstructure was used to investigate the fracture mechanism of the K4169 superalloy in detail. Figure 11 shows the fracture surface morphologies of the samples following fracture at 3 and 4.5 kN. Under the 3 kN cyclic loading, the fracture extension rate decreases as the cyclic stress load increases. As the strain increases and the fracture growth rate increases, three distinct stages are easily distinguished.

The main causes of K4169 superalloy fracture are fatigue striations, fibrous stripes and cleavage facets, as shown in Fig. 11. The dimple is encircled by a tear band that is essentially parallel to the direction of stretching but has a nonuniform height. On the fracture surface, however, microcracks are formed. The majority of K4169 superalloy fractures are caused by ductile deformation. Under the 3 kN cyclic loading, the fatigue fracture indicates that the fractures emerge from the manufactured cracks (Fig. 11(a)). Fatigue striations parallel to the fibrous striations are observed in the area where the fatigue fracture propagates, representing the location of the crack tip. The fibrous stripes, which stem from the crack, also exhibit the direction of fracture expansion. This finding suggests that the crack location is subjected to significant fatigue loading. In addition, dimple shapes are apparent when the

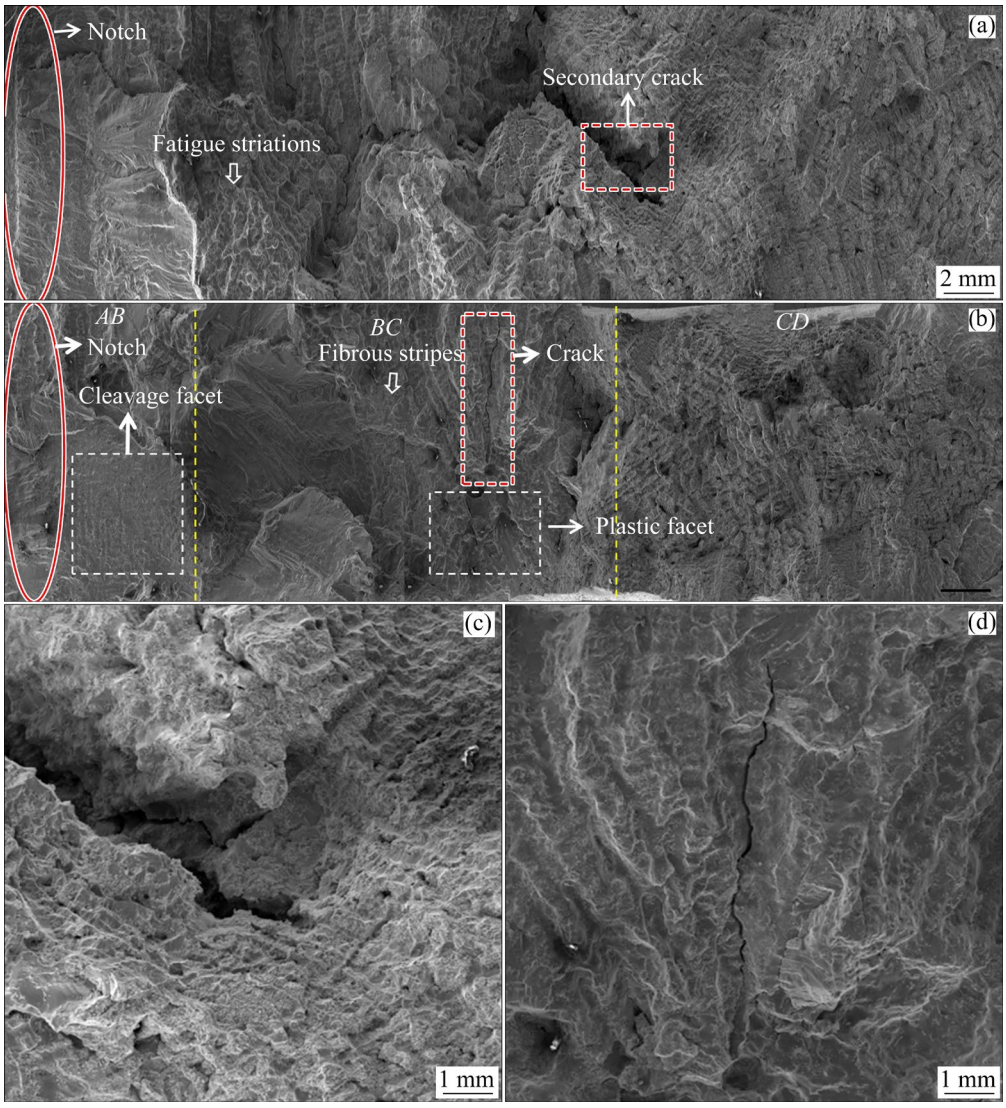

Fig. 11 Fracture surface morphologies of samples subjected to different cyclic loadings: (a, c) 3 kN; (b, d) 4.5 kN

fracture length exceeds a certain size. This reveals that instead of exhibiting crack destabilization expansion, the crack at this spot continues to develop. As shown in Fig. 11, for the sample under the 3 kN cyclic loading, in the steady extension stage, the mode of fracture is the ductile fracture.

Under the cyclic loading of 4.5 kN, according to the fatigue fracture, the prefabricated fracture has a cleavage facet (Fig. 11(b)). There is a height discrepancy between several developed cracks during the fatigue crack propagation process. As a result of this process, the alloy tears and eventually forms fibrous stripes. The secondary crack propagation on both fracture surfaces, which is formed along grain boundaries, is shown in Figs. 11(c, d). Furthermore, the cracks do not extend through the sample. The sample experiences unstable expansion as the cyclic loading is applied. A few plastic facets are present in the fracture, and the mode of fracture is the mixed ductile−brittle fracture.

4 Discussion

Through microstructural characterization of the post-service samples, it is observed that precipitated phases exist at the grain boundaries, which is detrimental to the mechanical properties of the alloy. To determine whether the cracks at the grain boundaries are enriched with precipitated phases, SEM micrograph and element distribution tests were conducted in the cracked region shown in Fig. 8(a). The analyses of the compositions of the precipitated phases at the fracture sites are shown in Fig. 12. In Fig. 12, the crack propagation path is followed by intergranular propagation. The white granular precipitated phases are separated around the cracks, and Nb and Mo are well highlighted in the element distributions. Nb is the main component of the Laves phase, and Mo weakens the properties of the alloy while facilitating its precipitation near grain boundaries. This location is rich in the Laves phase on both the left and right sides of the fracture. The existence of the Laves phase allows the setting of the requirements for crack propagation. Furthermore, it is evident that the Laves phase fracture demonstrates brittle fracture properties, and this fracture does not result from a build-up of plastic deformation [24].

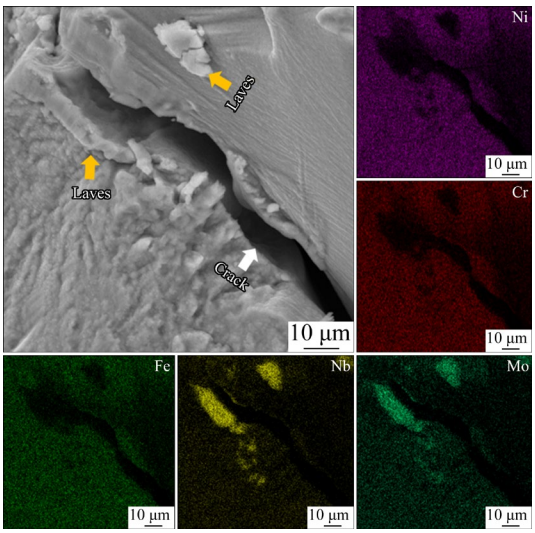

Fig. 12 SEM image and element distributions of sample under 3 kN cyclic loading

The most common method of cracking in K4169 superalloy is crystal cracking. The average grain size of the samples is approximately 800 μm, which is one of the contributing factors of crystal cracking. Larger grains result in higher strains at the grain boundaries due to high temperatures, which ultimately cause the boundaries to rupture. Figure 5 shows that the size interval of grain crushing is usually greater than 800 μm, there is less crushing at smaller sizes, and the large grains have a relatively high chance of breaking under stress. Figure 13 shows schematic diagrams of simulated

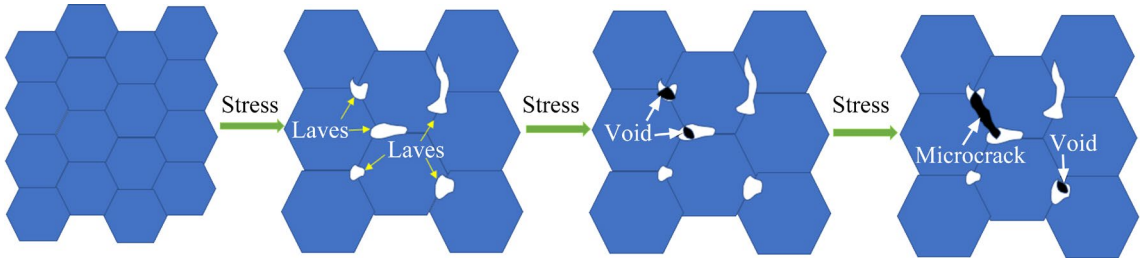

Fig. 13 Schematic diagrams of simulated cracking process of K4169 superalloy

cracking process of K4169 superalloy under cyclic loading at high temperatures. The conditions for the formation of the Laves phase are created by boundary breakage. Primary or secondary cracking can occur at the grain boundaries after the stress is applied due to the residual fine Laves phase [25]. When a hot-end component is used continuously, a crack easily forms and extends quickly, leading to the final breakage of the part.

The *a*–*N* curve shows that during the early stage of crack growth, prefabricated cracks begin to grow due to the impact of the applied load. The first crack undergoes plastic deformation at the tip before the crack propagation. However, the rate of crack propagation is slow until the fatigue fractures reach the stable expansion stage. A tiny cleavage facet is present at the early stage of fracture extension under the cyclic loading of 4.5 kN on the CT sample. Secondary cracking under both loadings exhibits ductile fracture characteristics during the stable extension stage.

5 Conclusions

(1) The grain size of K4169 superalloy significantly increases after service. When stress is applied, the Laves brittle phase precipitates at the grain boundary, and the grain orientation is increasingly inclined in the direction of the stress. The Laves phase becomes the site of the formation of voids and microcracks. The post-service sample exhibits the precipitation of needle-like δ phase and Laves phase, and the cracking mechanism is inter-granular propagation.

(2) There is a substantial positive association between the number of cycles and the fatigue crack propagation rate of K4169 superalloy. The entire alloy cracking process can be separated into three stages based on the *a*−*N* relationship curve, i.e., the initial slow extension stage, the middle steady extension stage, and the final destabilized extension stage.

(3) The initial type of fracture that develops when K4169 superalloy is subjected to loading is the ductile fracture. Secondary crack propagation occurs on the fracture surface. Furthermore, the fracture mode of the alloy changes from ductile fracture to brittle fracture when cyclic londing is applied.

CRediT authorship contribution statement

Song-jun WANG: Methodology, Data curation, Visualization, Writing − Original draft, Review & editing; **Jian-jun HE:** Methodology, Formal analysis, Visualization, Writing – Original draft; **Zhi-hui GONG:** Conceptualization, Writing – Review & editing; **Wei-ping LI:** Methodology, Writing – Review & editing; **Jun-gang YANG:** Writing – Review & editing; **Yu-hui CAI:** Data curation, Writing − Original draft, Supervision; **Ya-jun SHAO**, **Yue-xin DU** and **Cheng-wei YANG:** Data curation, Supervision.

Declaration of competing interest

The authors declare that they have no known competing financial interests or personal relationships that could have appeared to influence the work reported in this paper.

Acknowledgments

This work was financially supported by the National Natural Science Foundation of China (No. 51975200), and Hunan Provincial Innovation Foundation for Postgraduate, China (No. QL20220201).

References

[1] FIROZ R, BASANTIA S K, KHUTIA N, BAR H N, SIVAPRASAD S, MURTHY G V S. Effect of microstructural constituents on mechanical properties and fracture toughness of Inconel 718 with anomalous deformation behavior at 650 °C [J]. Journal of Alloys and Compounds, 2020, 845: 156276.

[2] WANG Qian, GE Shu-xin, WU Da-yong, MA Hai-kun, KANG Jie, LIU Meng, WANG Tao, NARAYANASWAMY B, SU Ru. Evolution of microstructural characteristics during creep behavior of Inconel 718 alloy [J]. Materials Science and Engineering: A, 2022, 857: 143859.

[3] CAO Shu-ting, YANG Ya-qian, CHEN Bo, LIU Kui, MA Ying-che, DING Lei-lei, SHI Jun-jie. Influence of yttrium on purification and carbide precipitation of superalloy K4169 [J]. Journal of Materials Science & Technology, 2021, 86: 260−270.

[4] YAZDANPANAH A, REVILLA R I, FRANCESCHI M, FABRIZI A, KHADEMZADEH S, KHODABAKHSHI M, DE GRAEVE I, DABALÀ M. Unveiling the impact of laser power variations on microstructure, corrosion, and stress-assisted surface crack initiation in laser powder bed fusion-processed Ni−Fe−Cr alloy 718 [J]. Electrochimica Acta, 2024, 476: 143723.

[5] FAYED E M, BRAILOVSKI V, JAHAZI M, MEDRAJ M. Stability of the microstructure and elevated-temperature mechanical properties of additively manufactured Inconel 718 superalloy subjected to long-term in-service thermal

cycling [J]. Materials Science and Engineering: A, 2022, 838: 142790.

[6] IZADI GHAHFEROKHI A, KASIRI-ASGARANI M, AMINI K, RAFIEI M, EBRAHIMI-KAHRIZSANGI R. Role of interlayer composition in microstructure and mechanical properties during TLP bonding of GTD-111/IN-718 superalloys [J]. Transactions of Nonferrous Metals Society of China, 2022, 32(3): 908−926.

[7] XIAO Guan-fei, JIANG Ju-fu, WANG Ying, LIU Ying-ze, ZHANG Ying, HUANG Min-jie. High temperature creep behavior of thixoformed nickel-based superalloy parts [J]. Materials Science and Engineering: A, 2021, 814: 141216.

[8] CHEN Ju-tian, LU Jun-xia, CAI Wang, ZHANG Yue-fei, WANG Yong-feng, JIANG Wen-xiang, RIZWAN M, ZHANG Ze. In-situ study of adjacent grains slip transfer of Inconel 718 during tensile process at high temperature [J]. International Journal of Plasticity, 2023, 163: 103554.

[9] TIAN Su-gui, SUN Hao-fang, JIN Ying. Investigation on γ' to γ'' transition in an IN718G superalloy during heat treatment, using first principle [J]. Materials Characterization, 2020, 162: 110168.

[10] XUE Hao, ZHAO Jing-qi, LIU Yong-kang, ZHANG Chun-xiang, LUO Jun-ting. δ-phase precipitation regularity of cold-rolled fine-grained GH4169 alloy plate and its effect on mechanical properties [J]. Transactions of Nonferrous Metals Society of China, 2020, 30(12): 3287−3295.

[11] WANG Wei-zhan, CHEN Zhi-gang, LU Wen-jie, MENG Fan-gao, ZHAO Tai-yong. Heat treatment for selective laser melting of Inconel 718 alloy with simultaneously enhanced tensile strength and fatigue properties [J]. Journal of Alloys and Compounds, 2022, 913: 165171.

[12] KONEČNÁ R, KUNZ L, NICOLETTO G, BAČA A. Long fatigue crack growth in Inconel 718 produced by selective laser melting [J]. International Journal of Fatigue, 2016, 92: 499−506.

[13] SCHLESINGER M, SEIFERT T, PREUSSNER J. Experimental investigation of the time and temperature dependent growth of fatigue cracks in Inconel 718 and mechanism based lifetime prediction [J]. International Journal of Fatigue, 2017, 99: 242−249.

[14] BACHE M R, EVANS W J, HARDY M C. The effects of environment and loading waveform on fatigue crack growth in Inconel 718 [J]. International Journal of Fatigue, 1999, 21: S69−S77.

[15] JEONG D H, CHOI M J, GOTO M, LEE H C, KIM S. Effect of service exposure on fatigue crack propagation of Inconel 718 turbine disc material at elevated temperatures [J]. Materials Characterization, 2014, 95: 232−244.

[16] RASHKOVETS M, KISLOV N, GUSHCHINA M, NIKULINA A, POPELUKH A, KLIMOVA-KORSMIK O. Phase composition and fatigue crack growth behavior of Inconel 718 under additive manufacturing [J]. Materials Science and Engineering: A, 2022, 851: 143595.

[17] WAN Hong-yuan, ZHOU Zhong-jiao, LI Chang-peng, CHEN Guo-feng, ZHANG Guang-ping. Enhancing fatigue strength of selective laser melting-fabricated Inconel 718 by tailoring heat treatment route [J]. Advanced Engineering Materials, 2018, 20(10): 1800307.

[18] TAN Xi-ping, ZHENG Chao-hui ZHOU Xi-yan, YAN Bin, SHI Meng-he, LEI Si-xiong, ZHOU Jian, WANG Qi-rong. Thermal fatigue behavior of K4169 Ni-base superalloy for thin-wall investment castings [J]. Special Casting & Nonferrous Alloys, 2018, 38(8): 880−883. (in Chinese)

[19] ZHU Xu-min, GONG Cong-yang, JIA Yun-fei, WANG Run-zi, ZHANG Cheng-cheng, FU Yao, TU Shan-tung, ZHANG Xian-cheng. Influence of grain size on the small fatigue crack initiation and propagation behaviors of a nickel-based superalloy at 650 °C [J]. Journal of Materials Science & Technology, 2019, 35(8): 1607−1617.

[20] YAZDANPANAH A, FRANCESCHI M, REVILLA R I, KHADEMZADEH S, DE GRAEVE I, DABALÀ M. Revealing the stress corrosion cracking initiation mechanism of alloy 718 prepared by laser powder bed fusion assessed by microcapillary method [J]. Corrosion Science, 2022, 208: 110642.

[21] DENG Guo-jian, TU Shan-tung, ZHANG Xian-cheng, WANG Ji, ZHANG Cheng-cheng, QIAN Xia-yi, WANG Yi-ning. Small fatigue crack initiation and growth mechanisms of nickel-based superalloy GH4169 at 650 °C in air [J]. Engineering Fracture Mechanics, 2016, 153: 35−49.

[22] SINGH S R, MOTE R G, MISHRA S K. The effect of microstructures and precipitates (γ', γ'', δ) on machinability of Inconel-718 nickel-based superalloy in turning process [J]. Journal of Manufacturing Processes, 2022, 82: 374−389.

[23] WANG Song-jun, HE Jian-jun, LI Wei-ping, GONG Zhi-hui, ZHOU Li-bo, YANG Jun-gang, CAI Yu-hui, DU Yue-xin. Microstructure analysis and cracking mechanism of aero-engine hot-end component K4169 superalloy based on in-situ EBSD test [J]. Journal of Alloys and Compounds, 2023, 960: 170781.

[24] LIU J H, VANDERESSE N, STINVILLE J C, POLLOCK T M, BOCHER P, TEXIER D. In-plane and out-of-plane deformation at the sub-grain scale in polycrystalline materials assessed by confocal microscopy [J]. Acta Materialia, 2019, 169: 260−274.

[25] LI Xiang-hui, ZHANG Yong, HOU Xue-qin, GU Huai-peng, CHEN Jing-yang, CAO La-mei. Effect of homogenization temperatures on the microstructure and stress-rupture properties of K4169 alloy [J]. Rare Metal Materials and Engineering, 2014, 43(1): 199−203. (in Chinese)

航空发动机用 K4169 高温合金的高温疲劳开裂机制及其在服役过程中的显微组织演变

王嵩钧[1]，何建军[1]，龚志辉[2]，李伟平[2]，杨俊刚[3]，邵雅君[3]，蔡宇晖[1]，杜悦欣[1]，杨铖伟[1]

1. 长沙理工大学 能源与动力工程学院，长沙 410114；
2. 湖南大学 机械与运载工程学院，长沙 410082；
3. 中国航发南方工业有限公司，株洲 412002

摘　要：通过疲劳裂纹扩展试验及显微组织表征研究了 K4169 高温合金在不同载荷下的裂纹断裂和裂纹扩展机理。研究结果表明，K4169 高温合金在服役后晶粒尺寸明显增大，存在针状 δ 相和 Laves 相析出现象，在 Laves 相富集处萌生出孔洞与微裂纹，为裂纹的扩展创造了条件。a–N (a 为裂纹长度，N 为循环次数)关系曲线显示，随着循环次数的增加，疲劳裂纹扩展率的变化经历了 3 个不同的阶段。在低应力循环载荷(3 kN)下，K4169 高温合金的断裂机制为韧性断裂。当应力增加到 4.5 kN 时，其断裂机制开始从韧性断裂转变为脆性断裂。在这两种应力状态下，显微组织中的裂纹扩展机制均为沿晶裂纹扩展，同时还发现在断裂裂纹处存在 Laves 相，与服役后合金的组织现象相吻合。

关键词：K4169 高温合金；高温疲劳；显微组织；裂纹扩展；航空发动机

(Edited by Wei-ping CHEN)